Interface Formation and Mn segregation of Directly Assembled La$_{0.8}$Sr$_{0.2}$MnO$_3$ Cathode on Y$_2$O$_3$-ZrO$_2$ and Gd$_2$O$_3$-CeO$_2$ Electrolytes of Solid Oxide Fuel Cells

Shuai He,[a,b] Kongfa Chen,[c] Martin Saunders,[d] Zakaria Quadir,[e] Shanwen Tao,[f] John T.S. Irvine,[g] C. Q. Cui,[a,*] and San Ping Jiang[a,b,h*]

[a] School of Electromechanical Engineering, Guangdong University of Technology, Guangzhou 51006, People's Republic of China

[b] Fuels and Energy Technology Institute & Department of Chemical Engineering, Curtin University, Perth, WA 6102, Australia

[c] College of Materials Science and Engineering, Fuzhou University, Fuzhou 350108, China

[d] Centre for Microscopy, Characterisation and Analysis, The University of Western Australia, Perth, WA 6009, Australia

[e] John de Laeter Centre & Department of Physics and Astronomy, Curtin University, Perth, WA 6102, Australia

[f] ~~School of Materials Science and~~ Department of Chemical Engineering, Monash University, Clayton, Victoria 3800, Australia

[g] School of Chemistry, University of St Andrews, Fife KY16 9ST, UK

[h] Faculty of Science, Health, Education and Engineering, University of Sunshine Coast, Maroochydore DC, Queensland 4558, Australia

Corresponding Author: cqcui01@qq.com (CQ Cui); s.jiang@curtin.edu.au (SP Jiang)

Abstract:

The establishment of intimate electrode/electrolyte interface is critical in solid oxide fuel cells (SOFCs), as it plays an essential role in the overall cell performance and durability. In the present study, Mn segregation and interface formation between directly assembled

La$_{0.8}$Sr$_{0.2}$MnO$_3$ (LSM) and yttrium-stabilized zirconia (YSZ) or gadolinium-doped ceria (GDC) are thoroughly studied using combined focused ion beam and transmission electron microscopy (FIB-TEM). In the case of LSM/YSZ and LSM/GDC electrodes, a significant reduction in the electrode ohmic resistance was found after cathodic polarization at 900°C and 500mAcm^{-2}, indicating the formation of an intimate interface. However, LSM particle starts to disintegrate at the electrode/electrolyte interface with increasing polarization time in the case of LSM/YSZ electrode. On the other hand, the LSM/GDC interface is very stable with negligible disintegration of LSM phase at the interface. Mn segregation from the LSM perovskite structure was identified under the influence of polarization, regardless of the electrolyte materials. The results demonstrate that nature of the electrolyte plays a critical role in the interface stability of LSM based electrodes under SOFC operation conditions.

Keywords: solid oxide fuel cells; direct assembly; LSM cathodes; YSZ and GDC electrolyte; interface; Mn segregation.

1. Introduction

Solid oxide fuel cells (SOFCs) are energy conversion devices to efficiently produce electricity from the chemical energy of a wide variety of fuels, such as hydrogen, natural gas, and hydrocarbons [1-4]. SOFCs are considered as environmentally friendly technologies with significantly less greenhouse gas emission when comparing to the coal combustion plants [5, 6]. Typical SOFC cells consist of Ni-yttria-stabilized zirconia (Ni-YSZ) cermet anodes, YSZ electrolyte and lanthanum strontium manganite (LSM) perovskite cathode. Generally, the ceramic components of the SOFC devices are pre-sintered at high temperature, e.g., ~1400°C for Ni-YSZ cermet anode and ~1150°C for LSM cathodes [7-9] to establish intimate electrode/electrolyte interface. SOFCs are typically operated at ~800°C, and the performance

of the cell greatly depends on not only the electrocatalytic activity of electrode materials, but also the establishment of intimate electrode/electrolyte interface [10-13].

LSM perovskite is one of the most commonly and widely investigated cathode materials due to its high electronic conductivity and excellent electrocatalytic activity for oxygen reduction reaction (ORR) at high temperature [9, 14, 15]. As LSM is predominantly an electronic conductor with negligible ionic conductivity, the ORR mainly occur at the triple phase boundary (TPB) where the oxygen, electrode and electrolyte meet. The formation of an intimate electrode/electrolyte interface is thus critical in determining the performance and durability of SOFC cells, since it provides a direct pathway for oxygen species migration from electrode to electrolyte. In the case of LSM cathode, the formation of convex contact rings on YSZ and GDC electrolytes surface is observed after the high temperature pre-sintering [12, 16-21]. On the other hand, the significant effect of cathodic polarization on the electrode/electrolyte interface was observed under the fuel cell operation conditions, such as the formation of micro-pores and dense layer at the interface [18, 22-24], the increased TPB length [12], and the change of the electrolyte morphology [20, 25]. Early studies show that polarization can broaden and flatten the edges of the contact rings and the significant topography change of the convex rings is most likely due to the incorporation of oxygen and/or the interdiffusion processes between LSM and YSZ electrolyte at the interface [17]. The microstructure change at the electrode/electrolyte interface after long-term cathodic polarization can also lead to a significant cell performance degradation. Appel et al.[23] reported that after the LSM-YSZ composite cathode based cell was polarized at 300 mAcm^{-2} and 1000°C for 2000 h, an increase in overvoltage exceeding 100% of the initial value was found. They assumed that the morphology changes at the interface due to pore formation and densification of the electrode layer are the main reasons for the increase in the polarization resistance during the stability test.

Recently, we have shown the feasibility of applying directly assembled electrode on electrolyte without requiring further high temperature sintering, and the formation of electrode/electrolyte interface induced *in situ* by cathodic polarization [26-35]. In the case of LSM electrode and YSZ electrolyte, the initial results indicate that the electrochemical performance of cathodic polarization induced interface is comparable to that of the conventional pre-sintered electrodes, though the topography of the interface is very different, i.e. the formation of convex contact rings for the thermally induced interface and contact clusters for the electrochemically induced interface[26]. Further detailed study of the electrochemically induced LSM/YSZ interface by Li et al.[29] reveals that the interface formation is accompanied by the pronounced decrease of ohmic resistance, particularly during the first few hours of polarization. The cathodic polarization induces the LSM/YSZ interface formation most likely due to the enhanced oxygen ion migration processes. Studies show that LSM is thermally compatible with YSZ and GDC electrolytes and the formation of lanthanum zirconate only occurs at a higher temperature of 1300 ºC in the case of LSM/YSZ but not in the case of LSM/GDC[21]. However, the evolution of the electrode/electrolyte interface under the influence of cathodic polarization as well as the fundamental understanding of the crystallographic and compositional changes of the polarization induced interface in the case of directly assembled LSM electrodes are still not clear at this stage.

In this paper, a comparative study was carried out on the electrochemical activity, interface formation and Mn segregation of the directly assembled LSM electrode on YSZ and GDC electrolytes using combined FIB-STEM technique. The results indicate that the electrochemical performance of directly assembled LSM/YSZ and LSM/GDC cells was greatly enhanced by the cathodic polarization, and the establishment of electrode/electrolyte hetero-interface is characterized by the periodic lattice plane matching, accompanied by the formation

of lattice mismatch distortion. The nature of the electrolyte shows a significant effect on the stability of the interface formed between LSM and YSZ/GDC electrolyte.

2. Experimental

2.1. Fabrication of LSM electrode and electrolyte supported cells with direct assembled electrode

La$_{0.8}$Sr$_{0.2}$MnO$_3$ (LSM) cathode powder was synthesized via sol-gel method, using La(NO$_3$)$_3$·6H$_2$O (99.9%, A.R., Alfa Aesar, UK), Sr(NO$_3$)$_2$ (99%, A.R., Sigma-Aldrich, US), Mn(NO$_3$)$_2$ (50 wt% solution, A.R., Alfa Aesar, UK) as raw materials, and anhydrous citric acid (99.5%, A.R., Chem Supply, Australia), ethylenediaminetetraacetic acid (EDTA, 99%, Acros Organics, Australia) and ammonia solution (28%w.w., Sigma-Aldrich, US) as complexing agents with a molar ratio of 1:1.5:1 (metal ions/citric acid/EDTA). Stoichiometric metal nitrates were blended with deionized water, and the calculated amounts of citric acid, EDTA and ammonia solution were subsequently added. The pH of the solution was adjusted to 7 and the solution was stirred on a hot plate until the dry gel was formed. The resultant gel powder was calcined at 1000°C for 2 h.

Electrolyte pellets were fabricated by die-pressing powders of 8 mol% Y$_2$O$_3$ doped ZrO$_2$ (YSZ, Tosoh, Japan) and Gd$_{0.1}$Ce$_{0.9}$O$_{1.95}$ (GDC, AGC Seimi Chemical Co Ltd), followed by sintering at 1450°C for 5 h. The pellets were approximately 1 mm in thickness and 18 mm in diameter. Pt paste (Gwent Electronic Materials Ltd., UK) was painted on the centre and ring of the YSZ electrolyte and sintered at 1100°C for 2 h as the counter and reference electrodes. The LSM cathode powder was thoroughly mixed with an ink vehicle (Fuel Cell Materials, US) at a weight ratio of 5:5 in an agate mortar to form a uniform cathode paste. The cathode paste was subsequently screen-printed on the other side of the electrolyte symmetrically opposite to

the Pt counter electrode and then dried at 100ºC for 2h to form the directly assembled cathode/electrolyte cells without further high temperature pre-sintering[36].

2.2. Characterization

Electrochemical performance was measured on a Zahner Electrochemical Workstation. Directly assembled LSM/YSZ and LSM/GDC cells were cathodically polarized at 750 ºC and 500mAcm^{-2} for 1 and 12h, and electrochemical impedance was measured under open circuit conditions in a frequency range of 0.1 Hz to 100 kHz with a signal amplitude of 20 mV. Air at a flow rate of 100 mL min^{-1} was supplied to the cathode side. Electrode ohmic resistance (R_Ω) was obtained from the high frequency intercept, and electrode polarization resistance (R_p) was obtained from the differences between the low- and high-frequency intercepts of the impedance curves.

The microstructure of the electrolyte surface in contact with LSM was examined by scanning electron microscopy (SEM, Zeiss Neon 40EsB, Germany). In order to examine the morphology of the electrolyte surface, the LSM coating was completely removed by HCl (32 wt%, Sigma-Aldrich, US), and in some cases, the electrode was partly peeled off to reveal the electrode/electrolyte interface. The topographic features of the acid cleaned electrolyte surface were examined by atomic force microscopy (AFM, Alpha 300 SAR, WITec GmbH, Ulm Germany) at intermittent contact mode. Electrolyte lamella in contact with electrode particle was lifted out and milled to around 70 nm in thickness using FEI Helios Nanolab G3 CX Dual Beam Focused Ion Beam - Scanning Electron Microscope (FIB-SEM, Helios Nanolab G3 CX, FEI company, US) with Ga$^+$ ion source. The elemental mapping and microstructural micrographs were obtained on the FIB milled sample using a high angle annular dark field scanning transmission electron microscopy (HAADF-STEM, FEI Titan G2 80-200 TEM/STEM with ChemiSTEM Technology, US) at 200 kV. The fast Fourier transform (FFT)

images were extracted using TEM Imaging & Analysis software (TIA, FEI Company, US) to examine the diffraction behavior of selected area, and inverse FFT (IFFT) simulations were performed on Gatan Digital Micrograph (Gatan Digital Microscopy Suite, Gatan Inc., US) to reconstruct the selected lattice planes using FFT images.

3. Results and Discussion

3.1 Electrochemical performance of directly assembled LSM/YSZ and LSM/GDC electrodes

Fig. 1 shows the electrochemical properties of the directly assembled LSM cathode on YSZ and GDC electrolytes after polarization at 900°C and 500 mAcm^{-2} for 12 h. The performance of the LSM/YSZ cell improved significantly after cathodic polarization, showing a typical activation behaviour for LSM cathode [9, 37-42]. For instance, R_p was significantly reduced from 60.0 Ω cm^2 to 0.8 Ω cm^2 and R_Ω decreased dramatically from 2.1 Ω cm^2 to 0.9 Ω cm^2 (Fig.1a) The cathode potential ($E_{cathode}$) also drops quickly under the influence of cathodic polarization, from its initial value of 1.3 V to ~0.9 V. For LSM/GDC cell, the electrochemical performance also experiences a significant decrease (see Fig. 1b). Initial R_Ω and Rp were 1.1 Ω cm^2 and 1.0 Ω cm^2, and decreased to 0.6 Ω cm^2 and 0.3 Ω cm^2, respectively after polarization for 12 h. The $E_{cathode}$ also decreases gradually from 0.55V to 0.45V. The significant decrease in the R_Ω for both LSM/YSZ and LSM/GDC cells implies the establishment of cathode/electrolyte interface under the influence of cathodic polarization, as in the case of pre-sintered LSM/YSZ and LSM/GDC cells, no change in R_Ω was observed after cathodic polarization [21, 29].

3.3 Microstructure of the polarization induced interface [s1]

The microstructure of the YSZ and GDC electrolytes surface in contact with LSM cathode particles before and after polarization is presented in Fig. 2 and Fig. 3. respectively For LSM/YSZ cell, the morphology of the electrolyte surface was greatly changed after the

polarization at 900°C and 500 mAcm^{-2} for just 1 h, and the formation of ring-shaped contact marks was observed (Fig. 2b). In the contact rings, a considerable number of particles with a dimension of 28.8 ± 8.4 nm were found, indicating the possible disintegration of the LSM cathode under the influence of polarization. From Fig. 2a, it appears that the dimension of the contact rings closely corresponds to the structure of the cathode particles, and the cathode particles have a 1.57 ± 0.54 µm in diameter. After the polarization for 12 h, the ring-shaped contact marks continue to grow inwards, forming a number of craters on the electrolyte (Fig. 2c and d). The smooth electrolyte became dramatically roughened in the craters. The significantly transformed morphology of the electrolyte surface implies the possible reactions between LSM and YSZ under the influence of polarization. Matsui et al. also observed the significant microstructural change at the interface between pre-sintered LSM electrode and YSZ electrolyte and the increase of roughness of YSZ surface both in and out of contact with LSM particles with the increase of the polarization time at 1000 °C[40]. An increase in the length of three phase boundary was observed after polarization at 200 mA cm^{-2} for 5 h.

In the case of LSM/GDC cells, the change in the morphology of the GDC electrolyte is relatively small during the cathodic polarization (Fig. 3). For instance, after the cathodic polarization for 1 h, the morphology of the GDC electrolyte surface is still quite flat and smooth, and the formation of tiny ring-shaped contact marks is negligible, see Fig. 3a and b. After the cathodic polarization for 12 h, a number of small LSM particles were observed on the electrolyte surface, with a dimension of 0.33±0.19 µm, significantly ~~larger~~ smaller(?) than that of LSM particles, 1.88±0.88 µm. The morphology of the GDC electrolyte is changed, and the contact marks shown in Fig. 3b appear to grow and merge with each other, forming large-scale contact patterns (Fig. 3d). Although the microstructure of GDC electrolyte in contact with cathode also changes under the influence of polarization, it is much less significant as compared to the LSM/YSZ cells.

Fig. 4 shows the topography of the YSZ and GDC electrolyte surfaces in contact with LSM cathode measured by AFM. LSM electrodes were removed by acid treatment. In the case of LSM/YSZ cell, the morphology of the YSZ surface is greatly changed after the cathodic polarization for 1 h (Fig. 4a), indicated by the formation of convex contact rings with a dimension of 1.14 ± 0.54 µm. After the polarization for 12 h, the contact rings grow significantly, and the dimension of the rings increases to 1.80±0.71 µm. The AFM line scan across the edge of the contact rings reveals their depth profile of roughly 0.14±0.06 µm. The microstructure of the YSZ electrolyte in the contact rings is significantly roughened and a considerable number of clusters were formed, which may indicate the severe interaction between LSM cathode and YSZ electrolyte during the polarization. For the LSM/GDC cell, the electrolyte morphology is still flat and smooth without any noticeable changes after the polarization for 1h (Fig. 4d). Even after the polarization for a longer period (~12 h), the change of the GDC morphology is far less significant when comparing to the LSM/YSZ cell, as shown in Fig. 4e. Nevertheless, the formation of contact clusters was observed, and the average dimension of these clusters is 0.22±0.09 µm with the depth profile of 5.2±0.7 nm. The minor change of the GDC microstructure after long-term polarization may imply that the LSM cathode is more stable with GDC under the influence of polarization, consistent with the thermal compatibility studies [21].

Fig. 5 presents the LSM/YSZ and LSM/GDC interface lamella prepared by FIB, taking in the interface regions as shown in Figs. 2 and 3. The TEM images of the electrode/electrolyte interfaces clearly demonstrate the interface evolution under the influence of cathodic polarization. For example, in the case of LSM/YSZ cell, it appears that the LSM particle starts to disintegrate at the electrode/electrolyte interface after the polarization for 1 h, forming several discontinuous contact areas with the electrolyte. When the LSM/YSZ cell continues to be polarized for 12 h, the disintegration of the LSM cathode particle at the interface becomes

much more obvious (Fig. 5b). In the case of LSM/GDC cell, the disintegration of the LSM cathode particle seems to be much less significant. For instance, after the polarization for 1h, an intimate and void-free contact between cathode and electrolyte is established (Fig. 5c). The sharp and continuous LSM/GDC interface is still quite stable after the polarization for 12 h, very different to the LSM/YSZ interface.

3.4 LSM/YSZ interface

Fig. 6 shows the STEM-EDS and HRTEM results of directly assembled LSM cathode on YSZ electrolyte after polarization at $900^{\circ}C$ and 500 mAcm^{-2} for 1 h. From the STEM-EDS mapping shown in Fig. 6a, the element distribution for the two LSM cathode particles and YSZ electrolyte is presented. It appears that the bottom part of the cathode starts to disintegrate at the interface, and a clear presence of La and Mn is found in the disintegrated particles. It should be noted that there is a strong accumulation of Mn in one of the cathode particles, and it may be attributed to the Mn segregation under the influence of cathodic polarization. The contact between LSM and YSZ electrolyte seems to be established through the disintegrated cathode particles at the three-phase boundary (Fig. 6b), indicated by the significant decrease in R_{Ω}. The HRTEM images demonstrate an intimate contact between the small cathode particle and electrolyte with lattice planes meeting and matching at the interface. For example, the disintegrated LSM cathode particle can be identified by its periodic lattice arrangement of $\{202\}_{LSM}$ planes with a plane spacing of 0.22 nm [43, 44], while the YSZ electrolyte is characterized by the $\{111\}_{YSZ}$ lattice planes with plane spacing of 0.29 nm [45]. The orientation relationship between the two planes was found to be $\theta_{\{202\}LSM/\{111\}YSZ} = 46.9^{\circ}$, which is the angle between the $\{202\}_{LSM}$ and $\{111\}_{YSZ}$ lattice planes at the interface, and the mismatch factor (*f*) [46-49] for these two planes can also be calculated:

$$f = \frac{d_{\{111\}YSZ} - d_{\{202\}LSM}}{d_{\{111\}YSZ}} * 100\% = 24.1\% \qquad [1]$$

However, it should also be noted that the current examined interface and the orientation relationship between $\{202\}_{LSM}$ and $\{111\}_{YSZ}$ lattice planes may be different at different locations, as a result of the polycrystalline nature of both phase. Even though the observed LSM/YSZ interface is unique with a particular orientation of the two grains and their lattice adaptation, it reveals a main common feature of the interface [10].

The disintegration of LSM cathode particle becomes much more pronounced at the electrode/electrolyte interface after the polarization at 900°C and 500 mAcm^{-2} for 12 h, as shown in Fig. 7. The bottom portion of the LSM particle decomposed into a large number of small particles with the formation of voids in the bulk particle, and Mn segregation was also observed. In the disintegrated LSM particles, a strong accumulation of Zr and Y was detected, and their presence may imply the formation of La-Mn-Zr solid solution [50-53]. Although the formation of $La_2Zr_2O_7$ cannot be ruled out at this stage, the constant decrease of the electrode ohmic resistance of the cell during the polarization may indicate that the detrimental reaction between LSM and YSZ is negligible and insignificant [54]. The atomic geometry of the hetero-interface between the YSZ electrolyte and the disintegrated LSM particles shows the lattice plane matching of the two phases at the interface (Fig. 7b). For example, the YSZ phase has been identified by its $\{220\}_{YSZ}$ planes with a spacing of 0.18 nm, and the LSM phase can be characterized by its $\{202\}_{LSM}$ planes with plane spacing of 0.22 nm. The orientation relationship between the two examined planes was found to be $\theta_{\{202\}LSM/\{220\}YSZ} = 50.0^{o}$ with a lattice mismatch factor of $f = 18.2\%$. The FFT diffractogram of the electrolyte shows a typical cubic YSZ structure [45, 55], while for the LSM particle, it appears to be an overlap of two sets of same patterns at different orientation. This clearly indicates the overlap of two disintegrated LSM particles. Also, the abrupt image contrast change at the LSM/YSZ interface is obvious, most likely due to the strain effect resulted from the lattice mismatch of the heterogeneous phases [56-59]. The mismatch strain and the lattice misfit are usually relaxed

and accommodated by the occurrence of misfit dislocations [60-62], e.g. lattice plane distortion and bending at the interface, as indicated in Fig. 7.

Mn segregation has been studied on the LSM electrodes. Chen *et al*.[63] studied the interface reactions between LSM cathode and YSZ electrolyte in different atmospheres at 1000°C and found that Mn segregation is more pronounced at low oxygen partial pressure. This is consistent with that reported by Nishiyama [64], in which the oxygen potential gradient developed in the manganite was considered to give rise to the similar gradients in chemical potential of manganese, providing a driving force for manganese oxide segregation at the surface. Liu *et al*.[65] studied the influence of water vapour on the degradation behaviour of LSM based cells and observed an enrichment of Mn_2O_3 and Mn_3O_4 nano-particles (~100nm in size) on the electrode surface by STEM-EDS mapping after the cell was exposed to 20 vol.% humidified air and operated at 800°C for 200 h. We also observed a clear formation of Mn-rich phase, possibly Mn_3O_4 in the LSM electrode after the LSM-YSZ cell was subject to a current load of 500 mAcm^{-2} at 1000°C for 2543 h[66].

3.5 LSM/GDC interface

The influence of cathodic polarization on the interface of directly assembled LSM/GDC cells was also investigated and the results are shown in Fig.8. The STEM-EDS element mapping demonstrates the element distribution at the cathode/electrolyte interface after polarization at 900°C and 500 mAcm^{-2} for 1 h (Fig. 8a). Different from that observed for LSM/YSZ cell, no Mn segregation was observed. An intimate LSM/GDC interface was established after the polarization for 1 h with a high level of periodicity and symmetry the LSM/GDC interface, free of voids or amorphous phases (Fig.8b). The GDC electrolyte can be characterized by its {111}$_{GDC}$ planes with plane spacing of 0.31 nm, while LSM cathode can be identified by {110}$_{LSM}$ lattice planes with a spacing of 0.27 nm. The orientation relationship of these two

planes was found to be $\theta_{\{111\}GDC/\{110\}LSM} = 11.0^\circ$ with $f = 12.9\%$. Similar to the LSM/YSZ interface, the lattice plane distortion was also observed (indicated by the red arrows in Fig. 8b). Nevertheless, the observed lattice distortion only exists locally at the interface region without propagating into the electrode or electrolyte bulk. The formation of such misfit dislocations does not impede the incorporation of O^{2-} from cathode into the electrolyte, supported by the improved electrochemical performance during the cathodic polarization. This is consistent with that reported in the literature [21, 67, 68]. For example, Pergolesi et al [67] fabricated CeO_2 and YSZ biaxially textured epitaxial thin film using pulsed laser deposition method, and found that the hetero-interfaces are not uniform but significantly strained, yet no detectable contribution to the oxygen transport properties can be found.

The directly assembled LSM on GDC electrolyte cell was also polarized at $900^\circ C$ and 500 mAcm^{-2} for 12 h. LSM particles were in good contact with GDC electrolyte and the disintegration of LSM phase at the interface is much less significant as compared to that of LSM/YSZ cell under the identical polarization conditions (Fig.9a). Similarly, Mn segregation from the LSM cathode particle was observed, without contacting the GDC electrolyte. The negligible disintegration of LSM particle as well as the relatively small change of GDC microstructure in contrast to the LSM/YSZ cell may indicate that the solubility of La^{3+} and Mn^{2+} in GDC is much lower than that of in YSZ [51, 52, 69, 70]. The polarization induced LSM/GDC interface is sharp and abrupt, characterized by a high symmetry of lattice plane structure for both LSM and GDC phases, as shown by the HRTEM images of the LSM/GDC interface in Fig. 9b. From the FFT diffractogram images, the GDC electrolyte phase can be identified by its $\{220\}_{GDC}$ lattice planes with plane spacing of 0.19 nm, while LSM phase by the $\{012\}_{LSM}$ and $\{024\}_{LSM}$ planes with plane spacing of 0.39 nm and 0.19 nm, respectively. The orientation relationship of $\{220\}_{GDC}$ and $\{024\}_{LSM}$ was found to be 14.7° with lattice mismatch factor of 13%. The results indicate that the directly assembled LSM/GDC interface

is more stable than that of LSM/YSZ under the influence of cathodic polarization, consistent with the better thermal compatibility between LSM and GDC[21].

The Mn segregation from the LSM perovskite structure occurs in both cases of LSM/YSZ and LSM/GDC cells after cathodic polarization at $900^\circ C$ and 500 mAcm^{-2}. The STEM-EDS element mapping results reveals the manganese oxide was found to segregate from the LSM perovskite phase away from the GDC electrolyte region (Fig.10a). This may imply that Mn does not preferentially segregate at the electrode/electrolyte interface where oxygen reduction reaction occurs. The segregation manganese oxide can be identified by its $\{013\}_{MnOx}$ and $\{111\}_{MnOx}$ lattice planes with plane spacing of 0.29 nm and 0.25 nm, respectively (Fig.10b). The MnOx particle has an intimate contact with LSM cathode, free of voids or other phases, and a high level of symmetry and periodicity of lattice plane arrangement for both phases can be found at the MnOx/LSM interface. The interface geometry of MnOx/LSM is revealed as the matching of $\{111\}_{MnOx}$ and $\{110\}_{LSM}$ lattice planes with an orientation relationship of $\theta_{\{111\}MnOx/\{110\}LSM} = 40.7^\circ$ and a mismatch factor of 7.4%. The influence of Mn segregation on the performance degradation of the LSM/YSZ and LSM/GDC cells is not clear at this stage. [s2]Liu et al.[71] reported that Mn segregation occurs for the LSM-YSZ composite cathode and YSZ electrolyte after polarization at $850^\circ C$ and 1.76 Acm^{-2} for 1500 h and proposed that the Mn migration cannot be simply attributed to the element diffusion. It is likely due to the electro-transport induced element demixing [72, 73]. Hong *et al*.[72] studied the electrotransport-induced demixing behaviour in semiconducting spinel ferrite, $(Mn_xFe_{1-x})_3O_4$ in a constant current condition at $1200^\circ C$, and proposed that the degree of demixing is determined not only by the different diffusivity of the cations but also by their effective charges.

3.6 Effect of polarization on LSM/YSZ and LSM/GDC interfaces formation and Mn segregation

The results shown in the present study clearly indicate the significant effect of cathodic polarization on the interface formation and Mn segregation of directly assembled LSM/YSZ and LSM/GDC electrodes. The observation of the change of directly assembled cathode/electrolyte interface microstructure as well as the Mn segregation can be summarized as follows:

1. For directly assembled LSM/YSZ electrode, LSM cathode particle starts to disintegrate at the YSZ electrolyte interface in the initial stage of cathodic polarization (~1 h), and the discrete LSM particles form a number of contacts with the electrolyte. The atomic geometry of the LSM/YSZ interface is characterized by the matching of $\{202\}_{LSM}$ and $\{111\}_{YSZ}$ lattice planes, with a mismatch factor of 24.1%. The cathode/electrolyte interface is established with substantially reduced electrode ohmic resistance. There is a significant change in the morphology of the YSZ electrolyte surface in contact with LSM electrode, indicated by the formation of a large amount of ring shaped craters. With increasing polarization time (~12 h), the contact rings continue to grow in size, and the disintegration of the LSM particle becomes much more obvious at the interface. The presence of Zr and Y are found in those decomposed cathode particles, indicating the formation of solid solution of La-Mn-Zr phase. The LSM/YSZ interface can be identified by the matching of $\{202\}_{LSM}$ and $\{220\}_{YSZ}$ planes with a lattice mismatch factor of 18.2%. Nevertheless, the disintegration of LSM cathode particle at the LSM/YSZ interface does not significantly impede the oxygen transport process, as supported by the improved electrochemical performance after the cathodic polarization.

2. For directly assembled LSM/GDC electrode, the disintegration of LSM perovskite structure and change in the morphology of GDC electrolyte are much less significant, as compared to that of LSM/YSZ electrode. For example, in the initial stage of cathodic polarization (~1 h), an intimate LSM/GDC interface was formed without the

disintegration of LSM particles. The lattice structure for the LSM/GDC interface is characterized by a high level of symmetry and periodicity of the lattice planes of $\{110\}_{LSM}$ and $\{111\}_{GDC}$ with a mismatch factor of 12.9%. In contrast to the LSM/YSZ cell, the morphology of GDC electrolyte surface after polarization was smooth without any noticeable changes. With increasing polarization time (~12 h), the LSM/GDC interface remains intact and clean with negligible disintegration of LSM particles at the interface. The examined cathode/electrolyte interface is characterized by the match of $\{024\}_{LSM}$ and $\{220\}_{GDC}$ lattice planes with a mismatch factor of 1.3%. The change of the GDC electrolyte surface after the prolonged polarization is relatively small with the formation of a great number of small contact rings. As compared to the LSM/YSZ electrode, the negligible change of the GDC electrolyte microstructure as well as the disintegration of LSM particle at the interface may indicate that LSM and GDC are quite stable under polarization conditions, which is in good agreement with that reported in the literature [69]. The well-established LSM/GDC interface after polarization can also be reflected by the significantly reduced ohmic resistance, indicating the enhanced oxygen transport process.

3. For both LSM/YSZ and LSM/GDC electrodes, the Mn segregation from the cathode has been observed under the influence of the cathodic polarization. The segregated Mn particle exists as manganese oxide, and the segregation appears occurring randomly. The observed MnOx/LSM interface was found to be sharp and clean without any noticeable voids or amorphous phase formed at the interface. The atomic geometry of the examined interface can be identified by the match of $\{111\}_{MnOx}$ and $\{110\}_{LSM}$ lattice planes and by the mismatch factor of 7.4%. The Mn segregation may be related to the electrotransport-induced element demixing, which usually occurs in multi-component ceramic oxide materials. However, in the present study, the Mn segregation does not

result in any obvious performance degradation in both LSM/YSZ and LSM/GDC electrodes. However, the influence of Mn segregation on the performance stability of LSM based cells could be significant in long-term polarization conditions.

The current study also demonstrates that nature of electrolyte has a significant effect on the stability of the LSM/electrolyte interface. LSM on GDC electrolyte shows a much stable interface as compared to that of LSM on YSZ electrolyte under identical polarization conditions. Due to the fact that the directly assembled electrodes do not go through the high temperature sintering, the initial physical contact between LSM electrode and YSZ or GDC electrolyte is very low and limited. Consequently, the low contact area would result in the initial high R_Ω, 2.1 Ω cm^2 in the case of LSM/YSZ electrode and 1.0 Ω cm^2 in the case of LSM/GDC electrode. The high ohmic resistance will result in a much higher current density at the interface, leading to the localized sintering due to the Joule heat generated. The heat generated will sinter the interface and thus enlarge the contacts at the interface. This is supported by the significantly decreased R_Ω from 2.1 to 0.9 Ω cm^2 for LSM on YSZ electrolyte and from 1.0 Ω cm^2 to 0.3 Ω cm^2 for LSM electrode on GDC electrolyte after polarization at 900°C and 500 mAcm^{-2} for 12 h (Fig.1). However, the significant disintegration of LSM particles at the LSM/YSZ interface indicates the localized heat generated would be high at the LSM/YSZ interface, as compared to that at the LSM/GDC interface. The fundamental reason for the significance in the localized heat at the interface is probably related to the significant differences in the nature of the YSZ and GDC electrolytes, particularly their ionic and electronic conducting behaviour. YSZ is a pure oxygen ion conductor with the ionic conductivity in the range of 0.08-0.11 S/cm at 1000 ^{o}C [74, 75], while doped ceria such as GDC is a mixed ionic and electronic conductor with significantly higher conductivities (0.20-0.25 S/cm at 1000 ^{o}C) [76, 77]. The high ionic conductivity of GDC could reduce the electrode ohmic resistance and at the same time accelerate the oxygen migration and diffusion at the

interface between LSM and GDC.[s3] This is in fact supported by the much lower R_Ω and R_p values of the LSM/GDC electrode, as compared to that measured on LSM/YSZ electrodes before polarization (see Fig.1).

Fig. 11 shows a schematic diagram comparing the Mn diffusion and interface formation of pre-sintered[21] and directly assembled LSM/YSZ and LSM/GDC electrodes studied in this work. For the pre-sintered LSM/YSZ cell, the interface establishment after high temperature sintering is characterised by the formation of convex contact rings on the electrolyte, and the atomic geometry of the intimate electrode/electrolyte interface can be identified by a high level of symmetry, free of voids or any other phases. In addition, the Mn^{2+} and La^{3+} cations were found to diffuse towards the YSZ electrolyte, and a strong accumulation of cations was detected in the convex rings, which indicates a strong solubility of Mn^{2+} and La^{3+} in YSZ. While for the directly assembled LSM/YSZ electrode, the formation of electrode/electrolyte interface is also observed after cathodic polarization, supported by the significantly reduced electrode ohmic resistance. The surface morphology of the YSZ electrolyte has been changed as well, characterized by the formation of a considerable amount of contact craters. Although the disintegration of LSM cathode particle occurs at the interface under the influence of current load, the discrete contact between the disintegrated LSM particles and the electrolyte most possibly provides the oxygen migration paths. Similar to the LSM/YSZ cells, the pre-sintered LSM/GDC interface is also characterised by the formation of convex contact rings on the GDC electrolyte surface, while the cation diffusion was not detected in this case, most likely due to their low solubility in doped ceria. In the case of directly assembled LSM/GDC electrode, the establishment of intimate electrode/electrolyte interface was observed after the cathodic polarization, and the disintegration of LSM cathode particles is negligible, very different to that of LSM/YSZ electrode. There is also a change at the GDC surface morphology, but the change is much less significant as compared to that of LSM/YSZ electrode. The lattice structure

of the LSM/GDC interface is sharp and abrupt, and no voids or any other phases can be identified. MnO_x segregation on the electrode surface was observed on both directly assembled LSM/YSZ and LSM/GDC electrodes.

4. Conclusion

The directly assembled LSM/YSZ and LSM/GDC interfaces and their evolution formed under cathodic polarization were thoroughly investigated using combined FIB-TEM technique in the present study. The results indicate that in the case of LSM/YSZ cell, the cathodic current passage induces the cathode particle to disintegrate at the electrode/electrolyte interface, forming numerous discrete contact points with the electrolyte. The YSZ tends to interact with the disintegrated LSM particles under the influence of cathodic current, and the formation of La-Mn-Zr solid solution is observed. Nevertheless, the electrochemical performances of the LSM/YSZ were constantly improved under the cathodic polarization. For LSM/GDC cell, the initial polarization promotes the formation of clean electrode/electrolyte interface free of voids or solid solutions, leading to a gradual increase of the electrochemical performances. Further polarization results in a slight disintegration of LSM particles at the interface, which is much less significant than LSM/YSZ cell. In addition, the Mn segregation was observed for both LSM/YSZ and LSM/GDC cells under the effect of cathodic polarization, and its influence on the electrochemical performances of the cell is negligible. This study provides an insight into in-depth understanding of electrode/electrolyte interface formation and may also have profound technological implications on the design and development of new generation SOFC cathodes.

References:

[1]   T.M. Gür, *Progress in Energy and Combustion Science* **54** (2016) 1.

[2]   A. Choudhury, H. Chandra, A. Arora, *Renewable and Sustainable Energy Reviews* **20** (2013) 430.

[3]   K. Chen, L. Zhang, N. Ai, S. Zhang, Y. Song, Y. Song, Q. Yi, C.-Z. Li, S.P. Jiang, *Energy & Fuels* (2015).

[4]   D. Papurello, R. Borchiellini, P. Bareschino, V. Chiodo, S. Freni, A. Lanzini, F. Pepe, G.A. Ortigoza, M. Santarelli, *Applied Energy* **125** (2014) 254.

[5]   N. Mahato, A. Banerjee, A. Gupta, S. Omar, K. Balani, *Progress in Materials Science* **72** (2015) 141.

[6]   S.C. Singhal, *Wiley Interdisciplinary Reviews: Energy and Environment* **3** (2014) (2) 179.

[7]   H. Moon, S. Kim, S. Hyun, H. Kim, *International Journal of Hydrogen Energy* **33** (2008) (6) 1758.

[8]   T. Fukui, S. Ohara, M. Naito, K. Nogi, *Journal of Power Sources* **110** (2002) (1) 91.

[9]   S.P. Jiang, *Journal of Materials Science* **43** (2008) (21) 6799.

[10]   M. Backhausricoult, *Solid State Ionics* **177** (2006) (19-25) 2195.

[11]   Y.L. Liu, A. Hagen, R. Barfod, M. Chen, H.J. Wang, F.W. Poulsen, P.V. Hendriksen, *Solid State Ionics* **180** (2009) (23-25) 1298.

[12]   T. Matsui, Y. Mikami, H. Muroyama, K. Eguchi, *Journal of The Electrochemical Society* **157** (2010) (12) B1790.

[13]   J.T.S. Irvine, D. Neagu, M.C. Verbraeken, C. Chatzichristodoulou, C. Graves, M.B. Mogensen, *Nature Energy* **1** (2016) (1) 15014.

[14]   S. Jiang, J.G. Love, L. Apateanu, *Solid State Ionics* **160** (2003) (1-2) 15.

[15]   A. Belzner, T. Gur, R. Huggins, *Solid State Ionics* **57** (1992) (3-4) 327.

[16]   T. Horita, T. Tsunoda, K. Yamaji, N. Sakai, T. Kato, a.H. Yokokawa, *Solid State Ionics* **152-153** (2002) 439.

[17]   S.P. Jiang, W. Wang, *Electrochemical and Solid-State Letters* **8** (2005) (2) A115.

[18]   T. Matsui, Y. Mikami, H. Muroyama, K. Eguchi, *Journal of Power Sources* **242** (2013) 790.

[19]   B. Hu, M. Keane, M.K. Mahapatra, P. Singh, *Journal of Power Sources* **248** (2014) 196.

[20]   T. Matsui, M. Komoto, H. Muroyama, K. Eguchi, *Fuel Cells* **14** (2014) (6) 1022.

[21]   S. He, K. Chen, M. Saunders, J. Li, C.Q. Cui, S.P. Jiang, *Journal of The Electrochemical Society* **164** (2017) (13) F1437.

[22]   J. Yang, H. Muroyama, T. Matsui, K. Eguchi, *Journal of Power Sources* **204** (2012) 25.

[23]   M.J. Jørgensen, P. Holtappels, C.C. Appel, *Journal of Applied Electrochemistry* **30** (2000) (4) 411.

[24]   M.A. Haider, S. McIntosh, *Journal of The Electrochemical Society* **156** (2009) (12).

[25]   K. Chen, S.S. Liu, N. Ai, M. Koyama, S.P. Jiang, *Phys Chem Chem Phys* **17** (2015) (46) 31308.

[26]   S.P. Jiang, *Journal of The Electrochemical Society* **162** (2015) (10) F1119.

[27]   K. Chen, N. Li, N. Ai, Y. Cheng, W.D. Rickard, S.P. Jiang, *ACS Appl Mater Interfaces* **8** (2016) (46) 31729.

[28]   M. Li, K. Chen, B. Hua, J.-l. Luo, W.D.A. Rickard, J. Li, J.T.S. Irvine, S.P. Jiang, *Journal of Materials Chemistry A* **4** (2016) (48) 19019.

[29]   N. Li, N. Ai, K. Chen, Y. Cheng, S. He, M. Saunders, A. Dodd, A. Suvorova, S.P. Jiang, *RSC Adv.* **6** (2016) (101) 99211.

[30]   N. Ai, N. Li, S. He, Y. Cheng, M. Saunders, K. Chen, T. Zhang, S.P. Jiang, *J. Mater. Chem. A* **5** (2017) (24) 12149.

[31]   N. Ai, N. Li, W.D. Rickard, Y. Cheng, K. Chen, S.P. Jiang, *ChemSusChem* **10** (2017) (5) 993.

[32]   N. Ai, S. He, N. Li, Q. Zhang, W.D.A. Rickard, K. Chen, T. Zhang, S.P. Jiang, *Journal of Power Sources* **384** (2018) 125.

[33]   N. Li, N. Ai, S. He, Y. Cheng, W.D.A. Rickard, K. Chen, T. Zhang, S.P. Jiang, *Solid State Ionics* **316** (2018) 38.

[34]   K. Chen, S. He, N. Li, Y. Cheng, N. Ai, M. Chen, W.D.A. Rickard, T. Zhang, S.P. Jiang, *Journal of Power Sources* **378** (2018) 433.

[35]   S. He, M. Saunders, K. Chen, H. Gao, A. Suvorova, W.D.A. Rickard, Z. Quadir, C.Q. Cui, S.P. Jiang, *Journal of The Electrochemical Society* **165** (2018) (7) F417.

[36]   K. Chen, N. Li, N. Ai, M. Li, Y. Cheng, W.D.A. Rickard, J. Li, S.P. Jiang, *Journal of Materials Chemistry A* **4** (2016) 17678.

[37]   S.P. Jiang, *Journal of Solid State Electrochemistry* **11** (2005) (1) 93.

[38]   S. Jiang, J. Love, *Solid State Ionics* **138** (2001) (3-4) 183.

[39]   W. Wang, S.P. Jiang, *Solid State Ionics* **177** (2006) (15-16) 1361.

[40]   T. Matsui, Y. Mikami, H. Muroyama, K. Eguchi, *J. Electrochem. Soc.* **157** (2010) (12) B1790.

[41]   M.A. Haider, S. McIntosh, *J. Electrochem. Soc.* **156** (2009) (12) B1369.

[42]   A.A. Vance, S. McIntosh, *J. Electrochem. Soc.* **155** (2008) (1) B1.

[43]   R. Moriche, D. Marrero-López, F.J. Gotor, M.J. Sayagués, *Journal of Power Sources* **252** (2014) 43.

[44]   A. Hammouche, E. Siebert, A. Hammou, *Materials Research Bulletin* **24** (1989) (3) 367.

[45]   C.M. Wang, S. Azad, V. Shutthanandan, D.E. McCready, C.H.F. Peden, L. Saraf, S. Thevuthasan, *Acta Materialia* **53** (2005) (7) 1921.

[46]   D. Wolf, S. Yip, *Materials Interfaces: Atomic-level Structure and Properties*, Springer Netherlands (1993).

[47]   S. Cazottes, Z.L. Zhang, R. Daniel, J.S. Chawla, D. Gall, G. Dehm, *Thin Solid Films* **519** (2010) (5) 1662.

[48]   Y. Ikuhara, *Journal of the Ceramic Society of Japan* **109** (2001) (1271) S110.

[49]   J.P. Locquet, D. Neerinck, L. Stockman, Y. Bruynseraede, I.K. Schuller, *Physical Review B* **38** (1988) (5) 3572.

[50]   Tatsuya Kawada, Natsuko Sakai, Harumi Yokokawa, M. Dokiya, *Solid State Ionics* **50** (1992) (3-4) 189.

[51]   M. Mori, T. Abe, H. Itoh, O. Yamamoto, G.Q. Shen, Y. Takeda, N. Imanishi, *Solid State Ionics* **123** (1999) (1-4) 113.

[52]   S. Ping Jiang, J.-P. Zhang, K. Föger, *Journal of the European Ceramic Society* **23** (2003) (11) 1865.

[53]   S.P. Simner, J.P. Shelton, M.D. Anderson, J.W. Stevenson, *Solid State Ionics* **161** (2003) (1-2) 11.

[54]   A. Mitterdorfer, L.J. Gauckler, *Solid State Ionics* **111** (1998) (3-4) 185.

[55]   U. Martin, H. Boysen, F. Frey, *Acta Crystallographica Section B Structural Science* **49** (1993) (3) 403.

[56]   O.I. Lebedev, G.V. Tendeloo, S. Amelinckx, H.L. Ju, K.M. Krishnan, *Philosophical Magazine A* **80** (2000) (3) 673.

[57]   C. Rentenberger, C. Mangler, S. Scheriau, R. Pippan, H.P. Karnthaler, *Materials Science Forum* **584-586** (2008) 422.

[58]   X.L. Wu, E. Ma, *Journal of Materials Research* **22** (2011) (08) 2241.

[59]   M. Sillassen, P. Eklund, N. Pryds, E. Johnson, U. Helmersson, J. Bøttiger, *Advanced Functional Materials* **20** (2010) (13) 2071.

[60]   F.K. LeGoues, *MRS Bulletin* **21** (1996) (04) 38.

[61]   F. Ernst, P. Pirouz, A.H. Heuer, *Philosophical Magazine A* **63** (1991) (2) 259.

[62]   A. Trampert, F. Ernst, C.P. Flynn, H.F. Fischmeister, M. Ru¨hle, *Acta Metallurgica et Materialia* **40** (1992) S227.

[63]   M. Chen, Y.L. Liu, A. Hagen, P.V. Hendriksen, F.W. Poulsen, *Fuel Cells* **9** (2009) (6) 833.

[64]   H. Nishiyama, *Journal of The Electrochemical Society* **143** (1996) (7).

[65]   R.R. Liu, S.H. Kim, S. Taniguchi, T. Oshima, Y. Shiratori, K. Ito, K. Sasaki, *Journal of Power Sources* **196** (2011) (17) 7090.

[66]   S. Jiang, W. Wang, *Solid State Ionics* **176** (2005) (13-14) 1185.

[67]   D. Pergolesi, E. Fabbri, S.N. Cook, V. Roddatis, E. Traversa, J.A. Kilner, *ACS Nano* **6** (2012) (12) 10524.

[68]   S. He, M. Saunders, K. Chen, H. Gao, A. Suvorova, W.D.A. Rickard, Z. Quadir, C.Q. Cui, S.P. Jiang, *Journal of The Electrochemical Society* **165** (2018) (7) F417.

[69]   L. Zhao, J. Hyodo, T. Ishihara, K. Sasaki, S.R. Bishop, *ECS Transactions* **57** (2013) (1) 1607.

[70]   V.P. Dravid, V. Ravikumar, M.R. Notis, C.E. Lyman, G. Dhalenne, A. Revcolevschi, *Journal of the American Ceramic Society* **77** (1994) (10) 2758.

[71]   Y.L. Liu, K. Thydén, M. Chen, A. Hagen, *Solid State Ionics* **206** (2012) 97.

[72]   J. Hong, H. Yoo, *Solid State Ionics* **113-115** (1998) (1-2) 265.

[73]   D. Monceau, M. Filal, M. Tebtoub, C. Petot, G. Petotervas, *Solid State Ionics* **73** (1994) (3-4) 221.

[74]   X.J. Chen, K.A. Khor, S.H. Chan, L.G. Yu, *Materials Science and Engineering: A* **335** (2002) (1-2) 246.

[75]   S.D. W., C.W. G., *Journal of the American Ceramic Society* **47** (1964) (3) 122.

[76]   K. Eguchi, T. Setoguchi, T. Inoue, H. Arai, *Solid State Ionics* **52** (1992) (1-3) 165.

[77]   H. Inaba, *Solid State Ionics* **83** (1996) (1-2) 1.
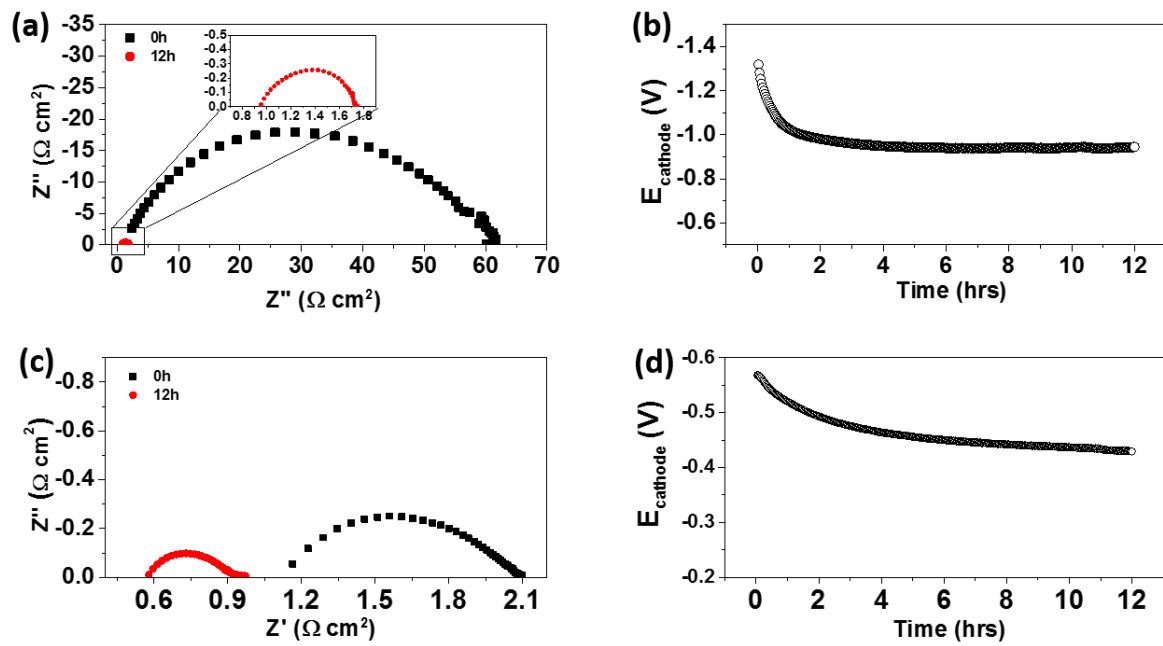
Figure 1. Electrochemical performance of directly assembled LSM cathode on (a,b) YSZ and (c,d) GDC electrolytes after polarization at 900ºC and 500 mAcm^{-2} for 12h.
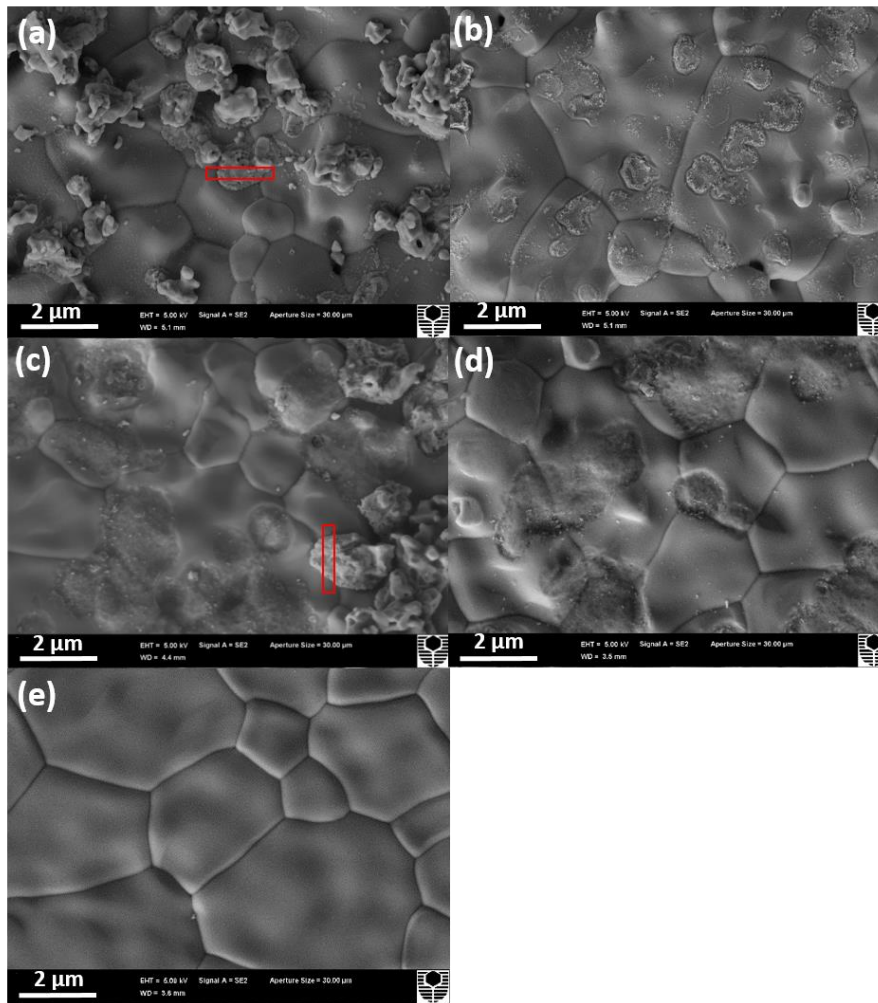
Figure 2. SEM micrographs of YSZ electrolyte surface after polarization at 900°C and 500 mAcm^{-2} for (a,b) 1 h and (c,d) 12 h. The LSM electrodes were removed (a,c) by stick tape and (b,d) by HCl treatment. The original YSZ electrolyte surface without LSM coating is given in (e). The red boxes indicate the locations of FIB milling.
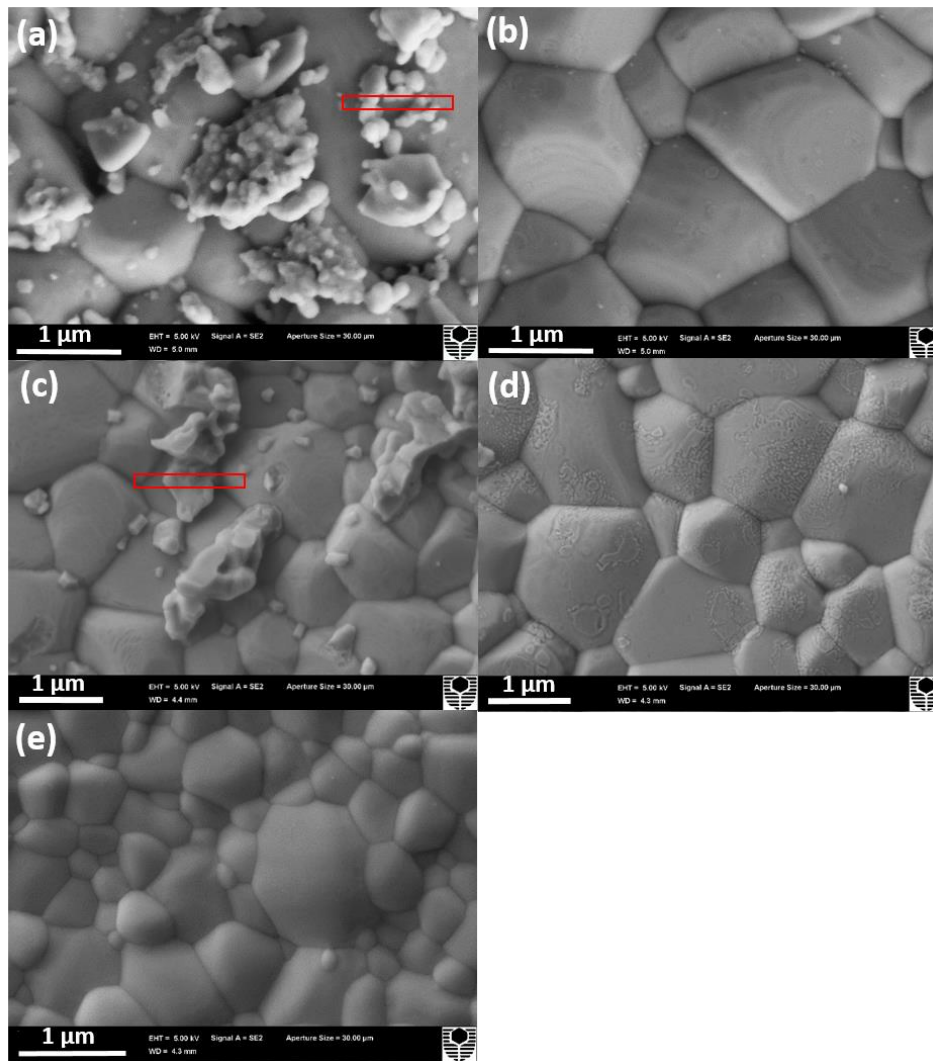
Figure 3. SEM micrographs of GDC electrolyte surface after polarization at 900℃ and 500 mAcm^{-2} for (a,b) 1 h and (c,d) 12 h. The LSM electrodes were removed (a,c) by stick tape and (b,d) by HCl treatment. The original GDC electrolyte surface without LSM coating is given in (e). The red boxes indicate the locations of FIB milling.
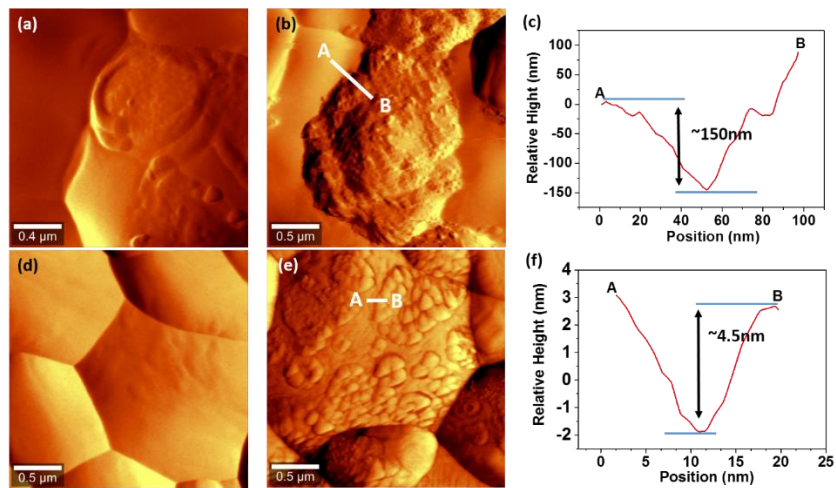
Figure 4. AFM micrographs and line scan of (a,b,c) YSZ and (d,e,f) GDC electrolyte surfaces after polarization at 900°C and 500 mAcm^{-2} for (a,d) 1 h and (b,e) 12 h. The LSM cathode was removed by HCl treatment.
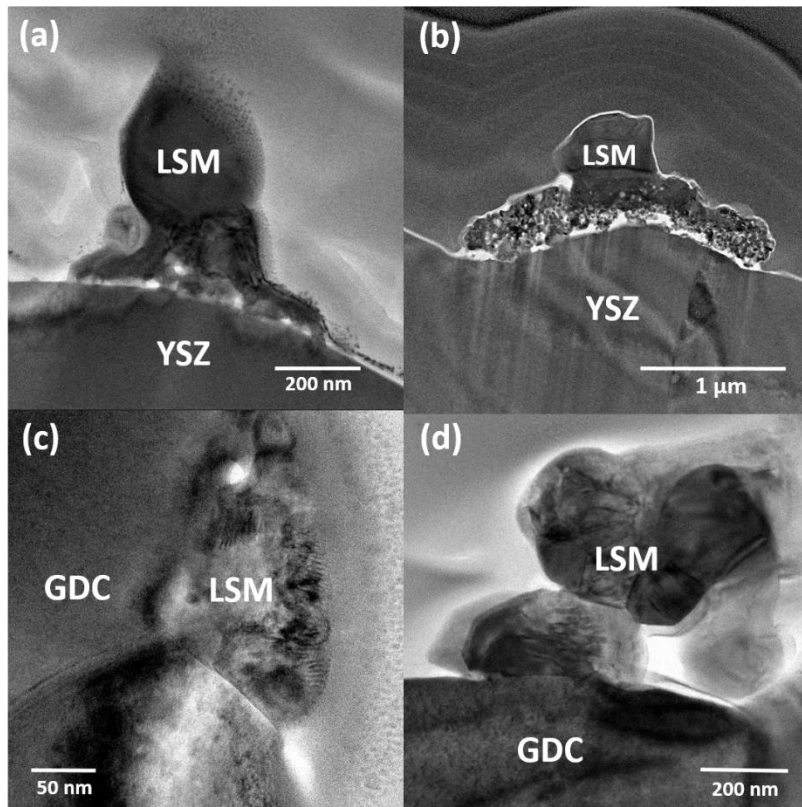
Figure 5. TEM micrographs of (a,b) LSM/YSZ interface and (c,d) LSM/GDC interface after polarization at 900°C and 500 mAcm^{-2} for (a,c) 1 h and (b,d) 12 h.
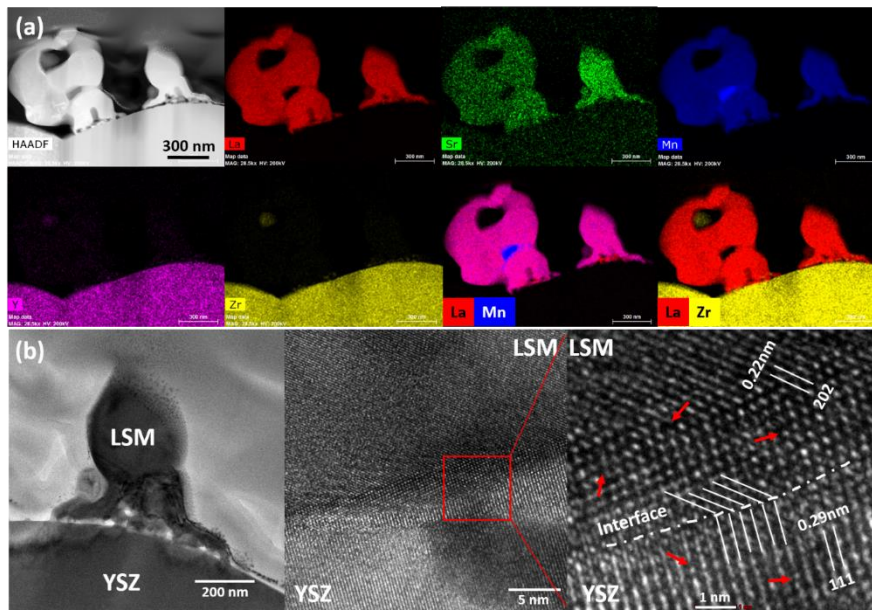
Figure 6. (a) STEM-EDS element mapping and (b) HRTEM micrographs of directly assembled LSM cathode on YSZ electrolyte after polarization at 900ºC and 500 mAcm^{-2} for 1 h. The red arrows indicate the locations of lattice distortion.
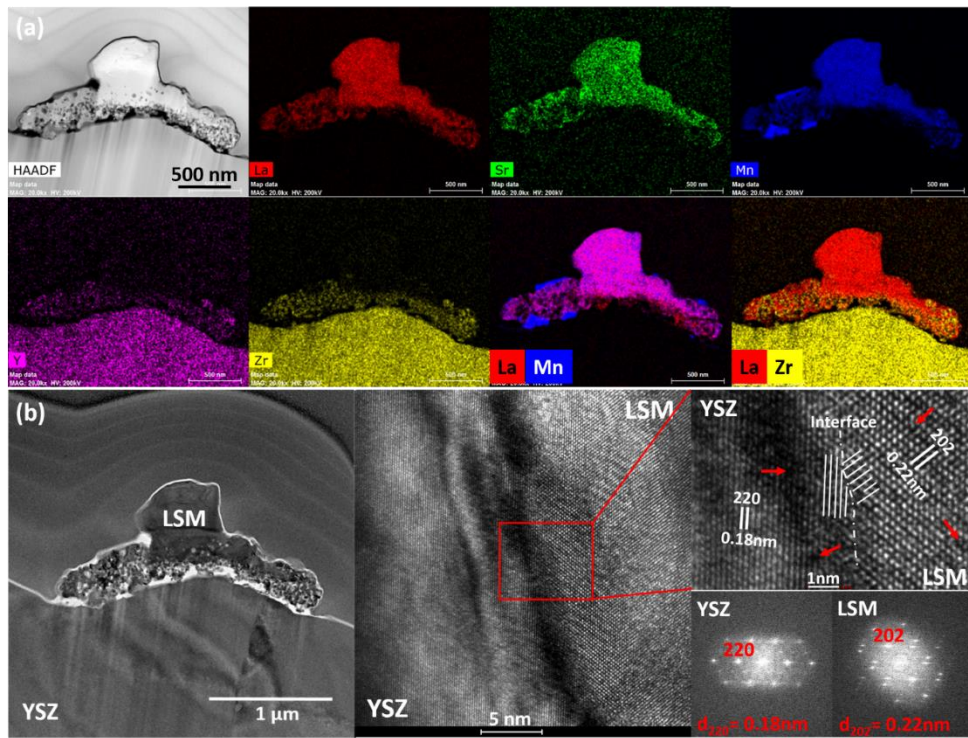
Figure 7. (a) STEM-EDS element mapping and (b) HRTEM micrographs of directly assembled LSM cathode on YSZ electrolyte after polarization at 900°C and 500 mAcm^{-2} for 12 h. The FFT shows the diffractograms of the YSZ and LSM phases. The red arrows indicate the locations of lattice distortion.
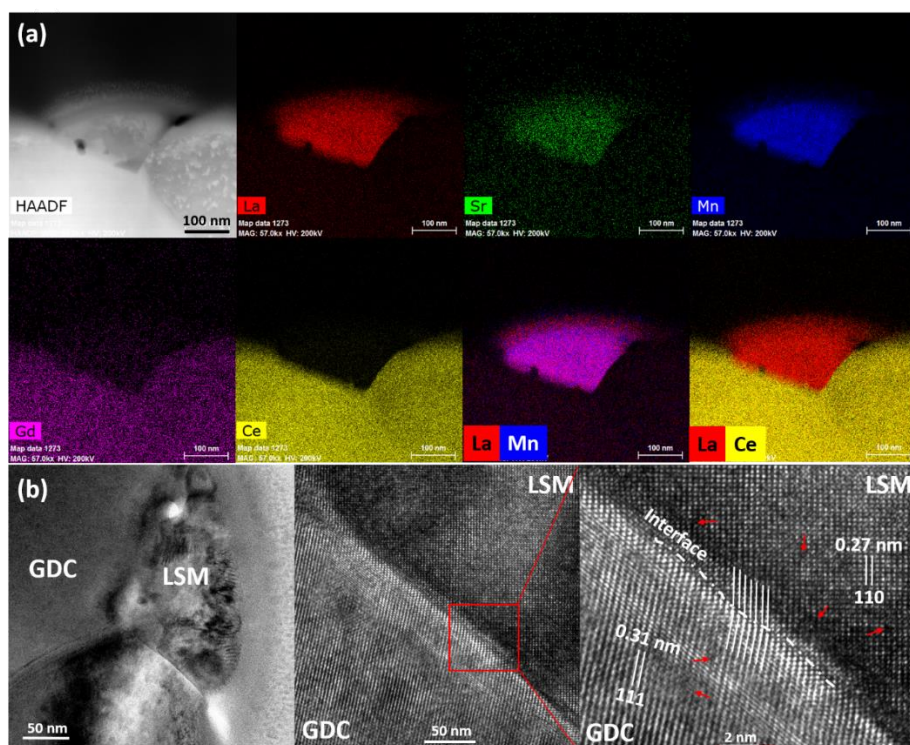
Figure 8. (a) STEM-EDS element mapping and (b) HRTEM micrographs of directly assembled LSM cathode on GDC electrolyte after polarization at 900°C and 500 mAcm⁻² for 1 h. The red arrows indicate the locations of lattice distortion.
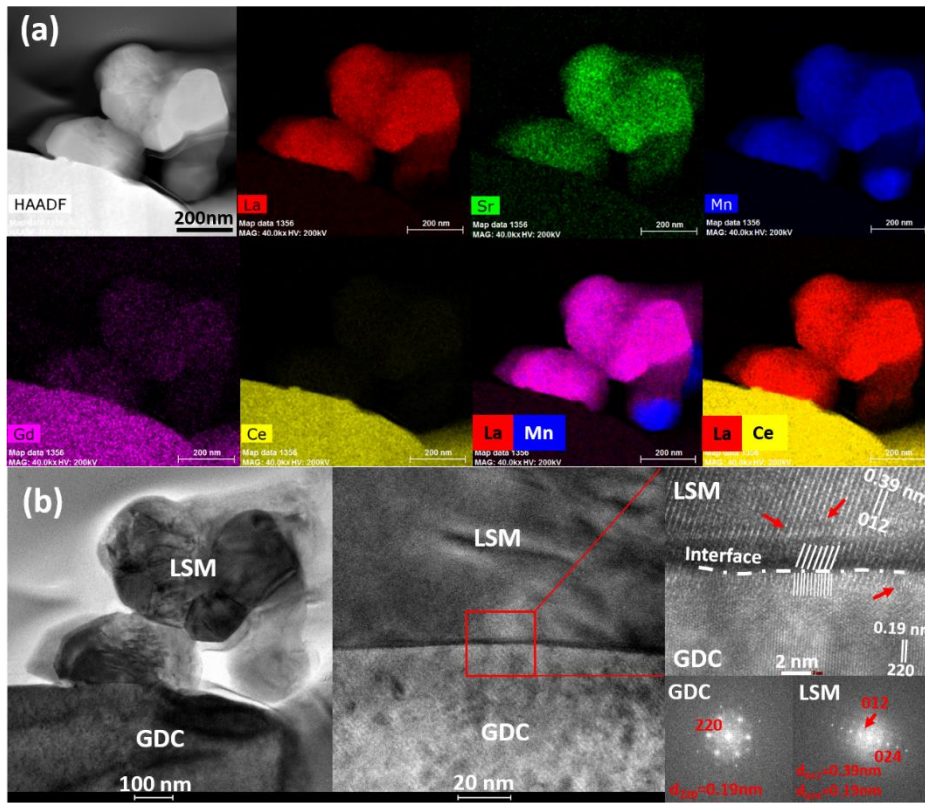
Figure 9. (a) STEM-EDS element mapping and (b) HRTEM micrographs of directly assembled LSM cathode on GDC electrolyte after polarization at 900°C and 500 mAcm^{-2} for 12 h. The red arrows indicate the locations of lattice distortion.
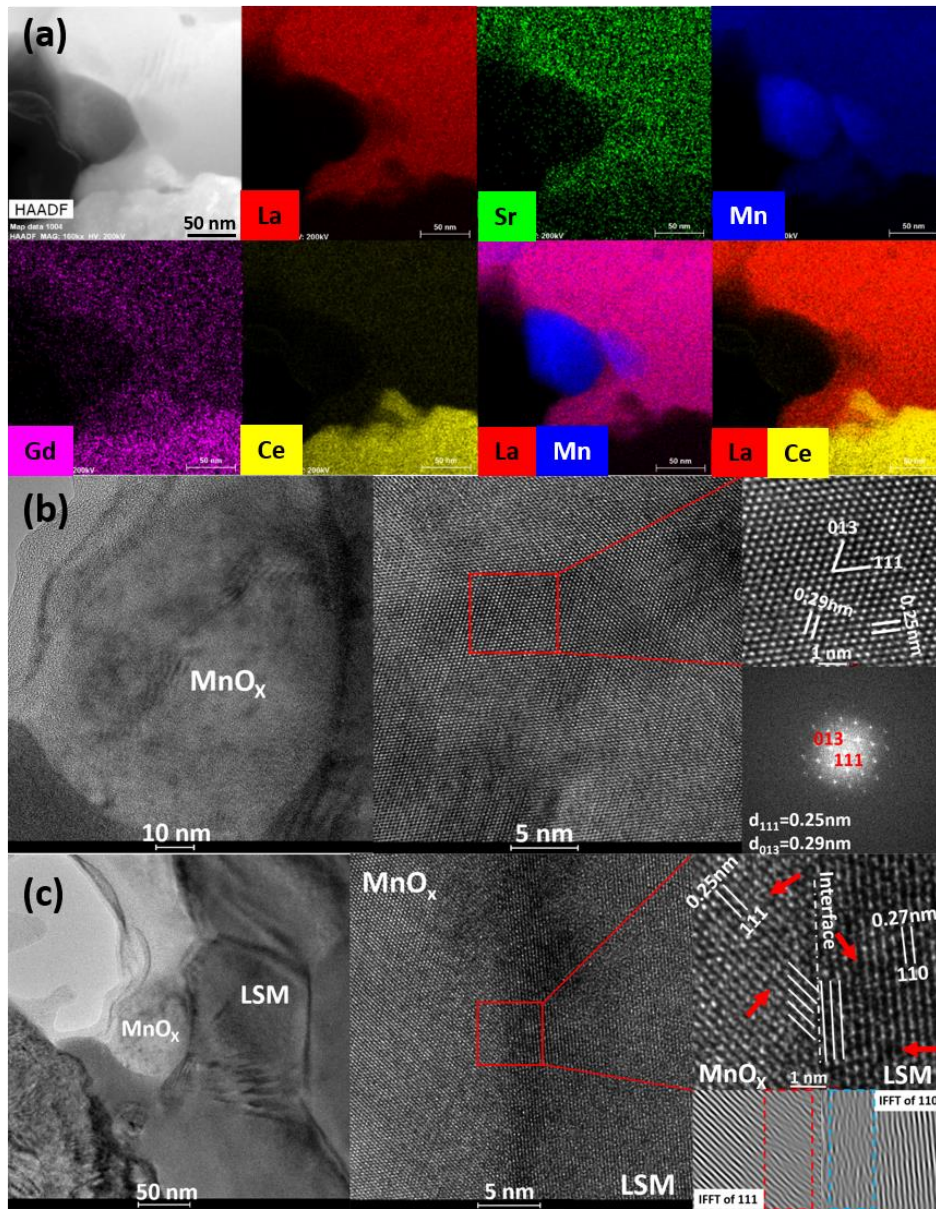
Figure 10. (a) STEM-EDS element mapping and HRTEM micrographs of (b) segregated MnOₓ particle and (c) MnOₓ/LSM interface after polarization at 900°C and 500 mAcm⁻² for 12 h on LSM/GDC. The red arrows indicate the locations of lattice distortion.
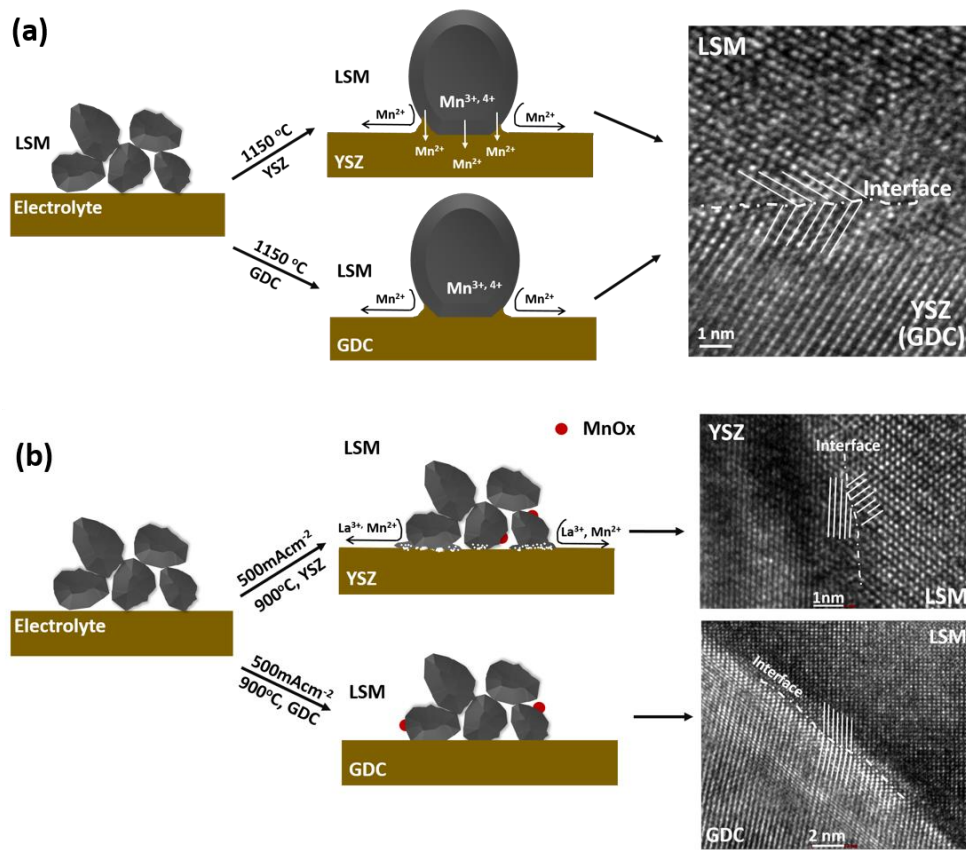
Figure 11. Schematic diagram showing the Mn diffusion and interface formation of (a) pre-sintered and (b) directly assembled LSM/YSZ and LSM/GDC electrodes.